RAPID COMMUNICATION

CELL TRACKING, SURVIVAL AND DIFFERENTIATION CAPACITY OF ADIPOSE-DERIVED STEM CELLS AFTER ENGRAFTMENT IN RAT TISSUE[†]

Mario F. Muñoz[1], Sandro Argüelles[2], Matias Guzman-Chozas[3], Remedios Guillén-Sanz[3], Jaime M. Franco[4], José A. Pintor-Toro[4], Mercedes Cano[2], Antonio Ayala[1]**

[1]Departamento de Bioquímicay Biología Molecular. Universidad de Sevilla. (Spain)

[2] Departamento de Fisiología y Zoología. Universidad de Sevilla. (Spain)

[3]Departamento de Nutrición, Bromatología, Toxicología y Medicina Legal. Facultad de Farmacia. Universidad de Sevilla. (Spain).

[4]Centro Andaluz de Biología Molecular y Medicina Regenerativa (CABIMER), Departamento de Señalización Celular. Sevilla (Spain)

**Correspondence:

Departamento de Bioquímica y Biología Molecular.

Facultad de Farmacia. Universidad de Sevilla.

C/. Tramontana s/n. 41012-Sevilla. Spain.

aayala@us.es

Abbreviations: ADSCs: adipose derived stem cells; ASCs: adult stem cells; BLI: Bioluminescence imaging; Luc: luciferase. MSCs: mesenchymal stem cells; PT: post-transplantation; SCs: stem cells; SN: substantia nigra; SVF: stromal vascular fraction; Ven: ventricle.

[†]This article has been accepted for publication and undergone full peer review but has not been through the copyediting, typesetting, pagination and proofreading process, which may lead to differences between this version and the Version of Record. Please cite this article as doi: [10.1002/jcp.26439]

Additional Supporting Information may be found in the online version of this article.

Received 30 June 2017; Revised 29 November 2017; Accepted 5 January 2018
Journal of Cellular Physiology

DOI 10.1002/jcp.26439

ABSTRACT

Adipose tissue is an important source of adipose derived stem cells (ADSCs). These cells have the potential of being used for certain therapies, in which the main objective is to recover the function of a tissue/organ affected by a disease. In order to contribute to repair of the tissue, these cells should be able to survive and carry out their functions in unfavorable conditions after being transplanted. This process requires a better understanding of the biology involved: such as the time cells remain in the implant site, how long they stay there, and whether or not they differentiate into host tissue cells. This report focuses on these questions. ADSC were injected into three different tissues (substantia nigra, ventricle, liver) and they were tracked *in vivo* with a dual GFP-Luc reporter system. The results show that ADSCs were able to survive up to 4 months after the engraftment and some of them started showing resident cell tissue phenotype. These results demonstrate their long-term capacity of survival and differentiation when injected *in vivo*.

Keywords: adult stem cells; mesenchymal stem cells; adipose tissue stem cells; bioluminescence, engraftment, differentiation.

INTRODUCTION.

One of the aspects of Regenerative Medicine is based on the regenerative capacity of adult stem cells (ASCs). It is now known that most of the tissues have specific populations of ASCs that allow them to renew or regenerate regularly (Burns et al., 2009; Hipp and Atala, 2008; Schaffler and Buchler, 2007; Teo and Vallier, 2010). Within the adult stem cell group are the mesenchymal stem cells (MSCs). The MSCs belong to the mesodermal lineage, which by a differentiation process leads to blood vessels, smooth muscle, mesothelium, the lymphatic system and connective tissue itself. These cells can be obtained from different organs including foetal liver, umbilical cord, and bone marrow (Kern et al., 2006; Wagner et al., 2005). Another important source is adipose tissue, which contains stem cells called adipose derived stem cells (ADSCs) (Gimble et al., 2007; Schaffler and Buchler, 2007; Trounson et al., 2011), which can differentiate into osteoblasts, chondroblasts and adipocytes, along with other progenitors of connective tissue. They also have the ability to differentiate into neurons, endocrine cells of the pancreas, hepatocytes, endothelial cells and cardiomyocytes (Schaffler and Buchler, 2007). Easy access to subcutaneous fat by liposuction, and its natural abundance, with no ethical problems associated with its use, makes adipose tissue an important source of MSCs (Casteilla et al., 2011; Poglio et al., 2010; Varma et al., 2007). Another advantage is that the proportion of MSCs is 500 times higher in adipose tissue than in bone marrow (Fraser et al., 2006; Fraser et al., 2008), so that a large number of cells can be obtained without many passes, decreasing the risk of chromosomal abnormalities induced senescence in the cultures (Tarte et al., 2010).

It is thought that stem cells (SCs) transplanted into damaged or aged tissues have a therapeutic or a restorative capacity. Once transplanted, these cells are used to rejuvenate the damaged tissues (Gimble et al., 2007; Han et al., 2015; Hipp and Atala, 2008). Obviously, these cells should be able to survive and carry out their functions in unfavorable conditions. Consequently, therapeutic application of stem cells in tissue repair requires a better understanding of the biology of these cells. Important questions are whether they remain in the engraftment site or not, how long they stay there, and whether they differentiate into host tissue cells. This information should be especially relevant in the case of potential ADSC therapies in chronic or degenerative diseases.

In order to address these issues, an animal model—rat —was used. After the rats were subjected to lipoplastia, ADSCs were isolated from their adipose tissue. Besides cell characterization, ADSCs were transfected with a dual GFP-Luc reporter to track the cellular

fate, i.e. distribution, localization, migration, and differentiation, after injection into different rat tissues. Cells were then visualized confirming their presence and possible differentiation into host phenotypes by immunofluorescence and immunohistochemistry. Our results showed that ADSCs were identified at the injection site up to 4 months, showing phenotypic markers of host tissue cells by then.

MATERIAL AND METHODS.

Animals.

All animal experiments were carried out according to the guidelines of the European Union Council (Directive 2010/63/UE), in agreement with Spanish regulations (BOE 34/11370, RD 53/2013) and were also approved by the University of Seville ethical committee. Male Wistar rats (300-500 g) were kept at a constant temperature of 22 ± 1ºC in a relative humidity of 60%, with a 12 hour light-dark cycle and free access to food and water.

Isolation of ADSCs.

ADSCs were isolated from the stromal vascular fraction, from adipose tissue, after enzymatic digestion with collagenase. The rats were anaesthetized with ketamine/xylazine (100/12.5 mg/kg). Adipose tissue removal was performed through a 2 cm bilateral inguinal incision. After surgery, the wounds were closed by suturing the muscle and skin with absorbable sutures. After removal, the excised fragment of adipose tissue was placed in a sterile container and washed 3 times with a phosphate buffered saline (PBS). The tissue was then transferred to a new sterile container with collagenase type I (0.9 U/ml), then incubated for 1 h at 37°C under shaking. The tubes were centrifuged for 10 min at 600 x g and the supernatants were discarded. Cells were resuspended in 10 ml of DMEM (Miltenyi Biotec, Germany) with 10% fetal bovine serum (FBS) (Gibco, USA) and 1% penicillin/streptomycin (Gibco). Cell suspension was passed through a 40 µm cell strainer (BD Bioscience, USA) and the filtrate was collected into a conical tube. Cell suspension was centrifuged for 10 min at 300 x g and the supernatant discarded. The pellet was resuspended in 5 ml of DMEM with 10% FBS and 1% penicillin/streptomycin.

For ADSCs isolation, we used a Magnetic-activated cell sorting (MACS©, Miltenyi Biotec) technology. Cell suspension was centrifuged at 300 x g for 10 min and the supernatant was completely aspirated. Cells were resuspended in 80 µl of Rinsing Buffer (2 mM EDTA, 0.1% BSA, PBS, pH 7.2) and 20 µl of Anti-CD90.1 Microbeads (Miltenyi Biotec) per 10^7 cells.

After 10 min at 4ºC, cells were washed with 1 ml of Rinsing Buffer and centrifuged at 300 x g for 10 min. The pellet was resuspended with 500 µl of Rinsing Buffer and cells were applied onto a MACS column previously placed in the magnetic field. The column was washed 3x3 ml with Rinsing Buffer. To obtain the labeled cells, the column was removed from the magnetic field and immediately flushed out with 5 ml of Rinsing Buffer with the help of a plunger. Finally, cells were centrifuged at 300 x g for 10 min and resuspended with culture media DMEM + FBS + antibiotics. Cells were incubated and maintained in a culture at 37ºC in 5% CO_2.

Phenotyping.

For ADSCs phenotyping, the samples were analyzed in a flow cytometer (FC500 Beckman Coulter), and expression of the markers was determined using the following monoclonal antibodies: anti-CD34-PE (SantaCruz), anti-CD45-PE (BD Pharmingen), anti-CD11b-PE (Bio-Legend), anti-CD29-APC (Miltenyi Biotec) and anti-CD90.1-FITC (Miltenyi Biotec). In this case the cells must be positive for CD90.1 and CD29 and negative for CD11b, CD34, and CD45.

Differentiation of ADSCs into osteoblast, adipocyte and chondroblast.

For the osteoblast differentiation assay, cells were cultured at a density of 4.2 x 10^3 cells/cm^2 with DMEM + FBS + 1% antibiotic. At 50-70% confluency, the medium being replaced by osteogenic differentiation medium (StemXVivo Media-R&D System). After 14-21 days osteoblasts were fixed with methanol and stained with NBT/BCIP (Sigma-Aldrich) to detect phosphatase alkaline.

For adipocyte differentiation assay, cells were cultured at a density of 2.1 x 10^4 cells/cm^2 with DMEM + FBS + antibiotics. At 100% confluency, the medium was replaced by adipogenic differentiation medium (StemXVivo Media-R&D System). After 10-14 days, adipocytes were fixed with methanol and stained with Oil Red O (Sigma-Aldrich) to detect lipid vacuoles.

For chondroblast differentiation assay, 250.000 cells in DMEM/F-12 Basal Medium (Sigma) were transferred to a conical tube. Cells were centrifuged at 200 x g for 5 min at room temperature. The medium was replaced by chondrogenic differentiation medium (StemXVivo Media-R&D System). After 21 days, the pellet was fixed with 4% paraformaldehyde in PBS for 1-2 h at room temperature. The pellet was frozen and cut into 5-10 µm-thick sections.

Immunofluorescence assay was performed by using specific primary antibody rabbit anti-aggrecan (RyD System) and anti-rabbit Alexa Fluor 488 as the secondary antibody.

Transfections, lentivirus production, and infections of rADSCs with a dual GFP-Luc reporter gene.

The GFP-Luc reporter system was based on the lentivirus pHRSIN-DUAL-GFP, kindly provided by Mary K. Collins (Windeyer Institute, London), which expresses two GFP genes under two different promoters. The GFP under the SFFV promotor was excised using the BamHI/NotI restriction sites and replaced by the luciferase gene, thus generating the pSIN-DUAL-Luc-GFP2 lentiviral vector. The insertion and orientation of DNA fragments were confirmed by restriction enzyme digestions and sequencing. For production of lentivirus, HEK293T cells were transfected with 13.5 µg of the lentiviral vector pSIN-DUAL-Luc-GFP2, plus 9 µg of the HIV packaging (pCMVDR8.91) and 4,5 µg of VSV-G (pMDG) plasmids by using Lipofectamine 2000 (Invitrogen). Lentivirus were harvested 48 h post transfection, passed through a 0.45 µm filter, and concentrated by ultracentrifugation at 100,000 x g for 90 min. For infection with the lentiviral stock, ADSCs cells were seeded in 25 cm^2 flask 24 h prior to infection. Lentiviral particles were used at a multiplicity of infection (MOI) of 5 and were added to the ADSCs culture in the presence of 8ug/ml of polybrene. Twenty-four hours after transfection, the cells were detached from the culture and GFP expression evaluated by flow cytometry.

Bioluminescence imaging (BLI) detects visible light emitted by cells labeled with luminescent enzymes, such as luciferase, when these enzymes react with their specific bioluminescent substrate (de Wet et al., 1985). BLI can noninvasively track luciferase-transduced cells implanted in living animals in real time. To assess the bioluminescence (BLI) activity, cells were detected in T25 flaks culture after addition of D-luciferin (Caliper Life Science) (150 µg/ml) prepared in PBS to the culture medium. Xenogen IVIS Lumina II imaging system and IVIS Imaging 4.2 software (Caliper Life Science, Alameda, CA, USA) were used to detect and analyze the BLI signal. Thus, the cells used in the experiments were rADSC-GFP-Luc^+.

rADSC-GFP-Luc^+ transplantation in central nervous system (CNS) and liver.

Animals were randomly divided into four groups (N=3), control being saline, 25.000 cells/µl, 2.0 µl and 4.0 µl injected into substantia nigra and ventricle, respectively and 3000

cells/µl, 100 µl injected into the liver. The rats were anesthetized with Isofluorane in O_2:N_2O (30:70%). 1% Monastral blue (Sigma-Aldrich) was added to the cell suspensions for monitoring the injection site. During surgery, the rats were fixed in a stereotaxic instrument (Stoelting, Dublin, Ireland). The skull was exposed through a small incision and a hole was drilled at the following coordinates relative to bregma: AP -2.5; L:-1.9; DV: -4.0 for ventricle (Ven), and AP -5.4; L: +1.8; DV: -8.3 for substantia nigra (SN). Cells were subsequently injected into the brain through a Hamilton neurosyringe 700/1700 (Sigma-Aldrich, USA) with a flow rate of 0,5 µl/min. In the case of liver, animals were anaesthetized with ketamine/xylazine (100/12.5 mg/kg) and cells were injected intraperitoneally using an insulin syringe (25G needle).

The days after transplantation, the animals were injected with D-luciferin intraperitoneally (150 mg/kg) 10 min before anesthesia. Xenogen IVIS Lumina II imaging system and IVIS Imaging 4.2 software (Caliper Life Science, Alameda, CA, USA) were used to detect and analyze the BLI signal. BLI images were normalized and reported as photons per second per square centimeter per steradian (p/s/cm^2/sr).

Immunofluorescence of rADSC-GFP-Luc$^+$.

After 4 months of the transplant, the animals were transcardially perfusion-fixed under terminal anaesthesia with saline followed by a paraformaldehyde solution containing 0.025% glutaraldehyde. Brains were post-fixed, cryoprotected, embedded and frozen in isopentane at –80°C. Thaw-mounted 20-µm coronal sections of SN, ventricle and liver were cut on a cryostat at −15°C and mounted on gelatine-coated slides. Sections were rehydrated in PBS for 10 min, and then blocked with PBS containing 1% normal serum for 1 h. The blocking solution was replaced with the primary antibodies diluted in the blocking solution containing 0.25% Triton-X-100, and the slides were then incubated in humid chamber overnight at 4-8ºC. For the immunofluorescence performed in SNC, the primary antibodies were rabbit anti-Luciferase (anti-Luc; Sigma-Aldrich.; 1:500) and mouse-derived anti-NeuN (anti-NeuN; Millipore; 1:500), meanwhile for immunofluorescence performed in liver the primary antibodies were mouse anti-Luciferase (anti-Luc; Sigma Aldrich.; 1:300) and rabbit-derived anti-asialoglycoprotein receptor 1/2 (anti-ASGPR1/2, Santa-Cruz; 1:300). NeuN is a neuronal antigen commonly used as a biomarker for neurons. ASGPR1/2 is expressed primarily on the sinusoidal surface of the hepatocytes.

After the incubation period, slides were washed three times in PBS and subsequently incubated with secondary antibodies in PBS containing 0.25% Triton-X-100 in a humid chamber for 2 h at room temperature in the dark. For the immunofluorescence performed in SNC, the secondary antibodies were AlexaFluor 488-conjugated goat anti-rabbit (Thermo Fisher; 1:250) and TexasRed-conjugated horse anti-mouse (Vector Laboratories; 1:250) whereas for immunofluorescence performed in liver the secondary antibodies were Fluorescein-conjugated horse anti-mouse (Vector Laboratories; 1:200) and AlexaFluor 647-conjugated goat anti-rabbit (Thermo Fisher; 1:250). Sections were washed three times with PBS for 10 min. To stain the nucleus we used ToPro3 (1:1000, Molecular Probes, Thermo Fisher) for SNC samples and Hoechst (1:1000, Sigma Aldrich) for liver samples. Both were added in the second wash. Finally, slides were coverslipped using fluorescent mounting medium (Dako). Fluorescence images were acquired using a Zeiss LSM 7 DUO confocal laser scanning microscope (Carl Zeiss Microscopy, Jena Germany) and processed using the associated software package (ZEN 2010; Carl Zeiss Microscopy). The immunofluorescence controls were performed as mentioned above but without primary antibodies.

Immunohistochemistry.

Animals were perfused and sections were prepared as described above. Sections were washed with PBS for 10 min and then treated with 0.3% hydrogen peroxide in methanol for 20 min, washed again, and incubated in a Tris buffer solution (TBS) containing 1% horse serum (Vector Laboratories, USA). Slides were drained and further incubated with the primary antibody rabbit-derived anti-Luciferase (1:500) in PBS containing 1% horse or goat serum and 0.25% Triton X-100 for 24 h. Sections were then incubated in a humid chamber for 2 h with biotinylated horse anti-rabbit immunoglobulin G (IgG, 1:200; Vector Laboratories). The secondary antibody was diluted in PBS containing 0.25% Triton X-100, and its addition was preceded by three 10-min rinses in PBS. Sections were then incubated with ExtrAvidin–Peroxidase buffer aqueous solution (1:100; Sigma- Aldrich). The peroxidase was visualized by performing a standard diaminobenzidine–hydrogen peroxide reaction for 5 min. Images were acquired using a digital camera (Olympus DP70) and processed using the associated software package for the camera (Olympus DPController and Olympus DPManager).

Cell number estimation.

Estimation of Luc-positive cell population within tissue sections was performed by using software that partitions, in an unbiased way, the section into a grid of equal-sized areas

(40 x 25 µm). Then, the cells were looked at inside the counting frame (image under 20 x lens objective), clicking the mouse to mark cells that fulfill the appropriate criteria. An average of 5 sections per animal were used for cell number estimation.

Statistical analysis.

Statistical analysis was performed using SPSS Statistic 20.0 (SPSS Inc. Chicago, IL, USA) where *P* values ≤0.05 were considered statistically significant. Results are expressed as mean ± SD. All the experiments showed non-normal distribution that was confirmed by the Shapiro-Wilk's test. One-Way ANOVA analysis followed by Kruskal-Wallis's test was used to identify differences between the groups. To show whether sample size could affect the statistical analysis, a post hoc power analysis was performed using G*Power statistical analysis software (Faul et al., 2007).

RESULTS.

ADSCs characterization.

The minimal criteria established by the International Society for cellular therapy (ISCT) including cell adherence, phenotyping and multipotentiallity were tested to confirm the population as MSCs.

In the adherence test, there was no evidence of the presence of cells in suspension after immunomagnetic isolation (Fig 1A), but some cells were observed in suspension when the SVF was cultured (Fig 1B). Any cell suspension disappeared with the frequent change of media in these SVF cultures. However, phenotyping tests showed that cells were isolated through the immunomagnetic process and presented markers according to guidelines of ISCT while the SVF cultures showed more varieties of positive markers. When cells were isolated by the immunomagnetic process they showed 98.0 ± 0.9% in CD29 and CD90 markers (Fig 1C); while in cells cultured directly from SVF, they showed a 24.7 ± 6.7% (Fig 1D). When lack of negative markers was determined, cells isolated by the immunomagnetic process had only <3% expression, while cells cultured directly from SVF showed hematopoietic markers at 30.3 ± 10.7% (CD11b,CD34,CD45). These results confirm that a more homogeneous cell population could be obtained by immunomagnetic isolation.

Multipotentiality of MSCs to differentiate *in vitro* into adipocytes, osteoblast and chondroblast was performed to confirm its multilineage differentiation capacity. Following 2 weeks of adipogenic differentiation, most of the cells in cultures showed intracellular accumulation of neutral lipids, as detected by Oil Red O staining (Fig. 1E). When the ADSCs were induced toward osteogenic cell populations, they were capable of presenting phosphate alkaline, as visualized by NBT/BCIP staining (Fig. 1E). Chondrogenic differentiation in 3D spheroid culture results in the formation of cartilage with a typical proteoglycan aggrecan extracellular matrix. Aggrecan was used as an indicator for cartilage formation and detected with Anti-Aggrecan conjugated with a secondary antibody, Alexa Fluor 488.

Labeling ADSCs with pSIN-DUAL-Luc-GFP2 reporter gene by lentivirus transduction to track cells *in vivo.*

To develop the imaging approach, ADSCs were labeled with the Luc-GFP2 dual reporter gene by lentiviral infection. Luc was used for *in vivo* BLI along with immunofluorescence for cell tracking in tissues, while GFP was used to find the percentage of ADSCs expressing the GFP-Luc reporter gene. The reporter gene was driven by a constitutive SFFV promoter for Luc and UBIQ1 for GFP (Fig 2A). The labeling efficiency was 68.71% based on the cytometric flow analysis of GFP-positive cells (Fig. 2B). Cells also showed a strong BLI signal during culture. However, when they were engrafted into the animals, BLI intensity diminished with time ($p=0.001$) (Fig 2C).

Distribution of labeled ADSCs after administration in different tissues.

To determine the survival of engrafted cells in different tissues, 1×10^5, 5×10^4 and 3×10^5 rADSCs-GFP-Luc cells were transplanted into the ventricle, substantia nigra and liver, respectively. The ventricle BLI signal declined up to background levels at 5-day (Fig 3A). In the SN group, BLI signal remained for only the first 4 days, and was decreased up to background levels at 5-day PT (Fig 3B). By contrast, rADSCs showed dispersed distribution within the liver after intraperitoneal transplantation. The liver BLI signal focused on the liver zone and gradually declined over time, retreating to background levels at 7-day PT (Fig 3C). No BLI signal could be detected in other organs.

Immunofluorescence detection after BLI signal loss.

The BLI signal *in vivo* declined and disappeared before 8 days in immunocompetent rats, in both the CNS and the liver. To determine if this loss of signal was due to an engraftment

rejection, an immunohistochemical visualization was performed 4 months later in those places where cells were transplanted. We observed that the cells survived the engraftment in spite of there not being any BLI signals. Immunofluorescence against luciferase in the ventricle revealed Luc-positive cells around the injection (Fig. 4A). The same results were obtained in SN (Fig. 4B & 4C). The presence of luciferase is according to viable cells. Nevertheless, immunofluorescence in the CNS, especially green fluorescence, could lead to false positives by autofluorescent biological compounds. For that reason it was convenient to confirm the same results by immunohistochemistry. Thus we also visualized Luc-positive cells by immunohistochemistry staining with DAB, in both ventricle (Fig 4D) and SN (Fig 4F). Fibroblast-like morphology, in Luc-positive cells, was detected around the injection in higher magnification images (Fig 4E & 4G).

Co-localization Luc with NeuN and ASGPR1/2.

Cells that express a xenoprotein, such as Luc, allow us to differentiate cells that are transplanted from any other resident cell. A double immunofluorescence in confocal microscopy was performed to verify whether ADSCs expressed other phenotypic markers in those tissues where they were transplanted. In this study, we proposed using two common makers, typical of each tissue; for the CNS, NeuN was used as a marker of nuclear neuron and ASGPR1/2 to identify hepatocytes.

The results in SN (Fig 5A) showed that there were Luc and NeuN positive cells (Fig 5B). However, when images were merged there were some cells positives for both markers (Fig 5C). Nonetheless, not all Luc-positive cells contained a positive NeuN nucleus. Furthermore the intensity of NeuN expression in Luc-positive cells was lower than in cells that were only NeuN-positive (Fig 5D; see white arrows). With regards to the ventricle (Fig 6A), we observed Luc and NeuN positive cells as well (Fig 6B); when images were merged, there were also cells positive for both markers (Fig 6C) and Luc-positive cells contained a positive NeuN nucleus.

In the same way as SN, in the ventricle, the intensity of NeuN expression in Luc-positive cells was lower (Fig 6D; see white arrows) than only the NeuN-positive cells (Fig 6E).

In liver we used ASGPR1/2 as a marker to identify hepatocytes. In those places where cells were engrafted in the liver (Fig 7A & 7B) the results showed the presence of Luc positive and ASGPR1/2 positive cells (Fig 7C & 7D), and when images were merged some cells were positive for both markers, mainly localized around the hepatic acinous (Fig 7E & 7F; see white

arrows). These results were due to only the specificity of primary antibodies, because controls did not express any signals (Supplementary Fig. 1).

Estimated cell population within tissue section.

Cells expressing both Luc and NeuN or Luc and ASGPR1/2 were estimated (Fig 8). In SN, we estimated 18.83 ± 5.39 Luc-positive cells/mm^2, but only 7.00 ± 1.32 cells expressed both markers. In the ventricle, there was a decrease in the estimated number of cells, which expressed both markers, but this was not statistically significant. However, we can appreciate how there are more Luc-positive cells/mm^2 (41.33 ± 9.29) than in SN. This is according to the number of cells that were transplanted in each tissue. In the liver we estimated 5.6 ± 3.78 of Luc-positive cells/mm^2, in spite of the number of engrafted cells being higher in the liver than in the other tissues.

DISCUSSION.

Adult stem cells (ASCs) present in tissues play an important role in the maintenance of health. In theory, these cells contribute to keeping tissues healthy by two mechanisms: they generate new cells or they participate in the repair of tissue damage. Depending on the tissue, ASCs are involved, or not, in both functions (Goodell and Rando, 2015). With age, the regenerative capacity of the SCs is reduced. In fact, the decline in genetic integrity of SCs plays an important role in the development of cancer during aging (Adams et al., 2015). Considering the biological functions of the SCs and the age-related changes occurring in these cells, which may underlie age-associated stem cell dysfunction, these cells have the potential of being used in the treatment of degenerative diseases and in the control of aging (Han et al., 2015). However, before applying SCs therapy to Clinical Medicine, it is necessary to understand many aspects of the biology of these cells, not just of the living tissues but also of those which are injected exogenously. In the case of resident cells, it is relevant to unravel the mechanisms related to the quiescence and self-renewal, which are frequently lost with age (Han et al., 2014; Kapur et al., 2015). In the case of the injected cells, there are some important key aspects to work out, such as understanding the biology of transplanted cells and their involvement within the biology of tissue repair (Li et al., 2015; Lin et al., 2010; Wang et al., 2009).

It is not known whether these cells have autonomy, how they interact with resident cells and the extracellular matrix and what may be their final biological fate. In addition, the niche can instruct these cells but these instructions can be disrupted with aging and degenerative

diseases (Adams et al., 2015; Arranz et al., 2014; Eggenhofer et al., 2014). Therefore, if input signals controlling tissue homeostasis are affected in aging and chronic diseases, many factors will affect optimal survival and function of transplanted cells. In addition to their differentiation capacity, ADSCs secrete many trophic factors and immunosuppressive molecules (Donega et al., 2014; Wang et al., 2009; Whone et al., 2012). Therefore, the therapeutic capacity and the ability of ADSCs to repair injured tissue is likely the result of both cell differentiation and paracrine alone or in combination (Kim et al., 2009; Ooi et al., 2015; Whone et al., 2012). Also, it is important to know if all tissues behave the same when they receive implants of SCs.

To understand how these cells behave once they are injected into tissues is crucial to have a system for cell tracking and assessment of survival and differentiation of the implanted cells. This report focus on these three aspects.

ADSCs obtained from adipose tissue were assessed for multipotency “in vitro”. Our results show that isolated cells met the criteria established by the ISCT in relation to plastic adherence, phenotyping and multipotentiality (Dominici et al., 2006). Therefore, the population of obtained cells can be considered as multipotent mesenchymal stem cells.

Having determined that these cells are stem cells and because no one knows for sure what happens to them after engraftment, we studied their *in vivo* behavior. There are several experimental methods for tracking cellular fate: i.e. distribution, localization, migration, and differentiation, all of them following engraftment. Thus, cells can be tracked by magnetic resonance imaging (MRI) (Wu et al., 2014), fluorescence imaging (FLI) (Yukawa et al., 2012), single-photon emission, computed tomography (SPECT) (Gholamrezanezhad et al., 2011), and Bioluminescence imaging (BLI) (Cao et al., 2016; Li et al., 2015). However, none of these techniques allow the tracking of cells for a long time. In this study, we addressed how long stem cells labeled with luciferase were able to emit bioluminescence after injection into different tissues. Our results show that, in all cases, the BLI signal was visible for only 4-8 days (Fig. 2 & 3). We also observed that there is only partial migration in the case of the liver.

However, the loss of BLI signals does not mean that the cells disappear or die. Using either immunofluorescence or immunohistochemistry staining, injected cells can be detected on the injection site up to at least 4 months after showing that ADSCs have the capacity for survival when injected *in vivo*. Although the injection site is not the original cell niche, these results show that cells are able to survive for a long period.

Another relevant aspect is whether stem cells are able to improve the health of diseased and injured tissue through stimulating endogenous repair mechanisms. In this sense, the question is whether the cell knows what to do under the influence of the microenvironment. Our results show that cells carrying luciferase expressed markers that are characteristic of the resident cells present in the injection site (Fig. 4-8), which are not expressed in ADSCs cultures prior to injection (data not shown). This suggests that ADSCs could differentiate into neurons or hepatocytes when they are surrounded by the specific tissue environment. Although there are *in vitro* studies showing that ADSCs can differentiate into neurons (Ying et al., 2012; Zhang et al., 2014); however, it remains to be elucidated whether these new neurons inside the tissues have the same functional characteristics as those of the native neurons. In the case of hepatocytes it has been reported that human ADSCs can differentiate into a hepatic lineage (Seo et al., 2005; Talens-Visconti et al., 2006). More importantly, ADCSs can be further induced by a microenvironment to transdifferentiate toward cells expressing albumin. These findings support further research into the use of *in situ* transplantation of ADSCs and to pave the way for using cell-based therapy in treating liver diseases (Chen et al., 2015; Yin et al., 2015).

In our case, ADSCs were injected into healthy tissue and this circumstance, perhaps, determined the proportion of cells that supposedly differentiate in the niche´s cell since we must bear in mind that a damaged niche could have a role in establishing a pro-regenerative milieu. Even then, we do not know if ADSCs are able to generate all cell types or just regenerate only those types of cells that were ablated. It is worth noting the role that the immune system has in regulating inflammation and tissue regeneration following injury, which in this case does not exist. Under these circumstances, the role of the immune system could be relegated to act, if so, against the presence of ADSCs (Coyne et al., 2006; Poncelet et al., 2007; Zangi et al., 2009).

In conclusion, our results show the “survival” of marked ADSCs, which were removed from their native environment and injected *in vivo*. These cells appear to survive for a long period of time when injected into different tissues and they also show some differentiation capacity *in vivo* even in the absence of damage.

FIGURE LEGENDS.

Figure 1. Microscopic image showing the adherence of rADSCs obtained from immunomagnetic isolation (**A**) or from SVF cultures directly (**B**). Flow Cytometry of cultured rADSCs obtained from immunomagnetic isolation expressed CD29/CD90.1 and negative markers (**C**). Cultured SVF directly expressed CD29/CD90.1 and negative markers (**D**). Multipotential differentiation to adipocytes was shown by Oil-O-Red staining, osteoblast differentiation was detected by Alkaline Phosphatase staining and chondroblast was determinate by anti-aggrecan antibody (**E**). Scale bar = 50 µm

Figure 2. Schema of lentivirus vector carrying reporter gene (GFP and Luciferase) (**A**). Flow cytometry analysis of rADSCs-GFP-Luc. *In vitro* bioluminescence imaging of rADSCs-GFP-Luc in culture (**B**). *In vivo* bioluminescence imaging of rADSCs-GFP-Luc transplanted in paws with 3 seconds of exposure (**C**). The values are the mean ± SD of three experiments with. **p < 0.01 versus 1^{st}-day. (1-β) > 0.8.

Figure 3. *In vivo* bioluminescence imaging of rADSCs-GFP-Luc transplanted in ventricle with 300 seconds of exposure (**A**), in SN with 500 seconds of exposure (**B**) and in liver with 300 seconds of exposure (**C**). The values are the mean ± SD of three experiments.**p < 0.01, *p ≤ 0.05 versus control. (1-β) > 0.8.

Figure 4. Immunofluorescence of Luc (green) in CNS (**A-C**). Immunohistochemistry of Luc staining with DAB. (**D-G**). Scale bar = 50 µm.

Figure 5. Confocal immunofluorescence microscopy of Luc (green), NeuN (red) and ToPro3 (blue) in SN. Injection zone (**A**). Images are shown separately (**B**) and merged (**C**). The region of interest was selected to show double positive cells (**D**). Scale bar = 50 µm.

Figure 6. Confocal immunofluorescence microscopy of Luc (green), NeuN (red) and ToPro3 (blue) in ventricle. Injection zone (**A**). Images are shown separately (**B**) and merged (**C**). The region of interest was selected to show double positive cells (**D-E**). Scale bar = 200 µm.

Figure 7. Immunofluorescence of Luc (green), ASGPR1/2 (red), and Hoechst (blue) in liver by confocal microscopy. Injection zone (**A-B**). Images are shown separately (**C-D**) and merged (**E-F**). Scale bar = 50 µm.

Figure 8. Luciferase and NeuN positive cell number in substantia nigra, ventricle, and ASGPR1/2 in liver. Cell number estimation was carried out as described in Materials and Method section. The values are the mean ± SD of three experiments. *$p \leq 0.05$ versus Luc+ cells in SN $(1-\beta) > 0.6$.

Supplementary Figure 1. Confocal immunofluorescence microscopy negative control of Luc (green), NeuN (red), ASGPR1/2 (red) and ToPro3/Hoechst (blue) in brain and liver. Scale bar = 50 μm.

REFERENCES

Adams PD, Jasper H, Rudolph KL. 2015. Aging-Induced Stem Cell Mutations as Drivers for Disease and Cancer. Cell Stem Cell 16(6):601-612.

Arranz L, Sanchez-Aguilera A, Martin-Perez D, Isern J, Langa X, Tzankov A, Lundberg P, Muntion S, Tzeng YS, Lai DM, Schwaller J, Skoda RC, Mendez-Ferrer S. 2014. Neuropathy of haematopoietic stem cell niche is essential for myeloproliferative neoplasms. Nature 512(7512):78-81.

Burns TC, Verfaillie CM, Low WC. 2009. Stem cells for ischemic brain injury: a critical review. J Comp Neurol 515(1):125-144.

Cao WJ, Wan DM, Li L, Wang C, Zhang SP, Liu CF, Xie XS, Sun H. 2016. [Clinical Study of Cytomegalovirus Infection and Preemptive Therapy after Allogenic Hematopoietic Stem Cell Transplantation]. Zhongguo Shi Yan Xue Ye Xue Za Zhi 24(4):1143-1148.

Casteilla L, Planat-Benard V, Bourin P, Laharrague P, Cousin B. 2011. [Use of adipose tissue in regenerative medicine]. TransfusClinBiol 18(2):124-128.

Coyne TM, Marcus AJ, Woodbury D, Black IB. 2006. Marrow stromal cells transplanted to the adult brain are rejected by an inflammatory response and transfer donor labels to host neurons and glia. Stem Cells 24(11):2483-2492.

Chen MJ, Lu Y, Simpson NE, Beveridge MJ, Elshikha AS, Akbar MA, Tsai HY, Hinske S, Qin J, Grunwitz CR, Chen T, Brantly ML, Song S. 2015. In Situ Transplantation of Alginate Bioencapsulated Adipose Tissues Derived Stem Cells (ADSCs) via Hepatic Injection in a Mouse Model. PLoS One 10(9):e0138184.

de Wet JR, Wood KV, Helinski DR, DeLuca M. 1985. Cloning of firefly luciferase cDNA and the expression of active luciferase in Escherichia coli. Proc Natl Acad Sci U S A 82(23):7870-7873.

Dominici M, Le Blanc K, Mueller I, Slaper-Cortenbach I, Marini F, Krause D, Deans R, Keating A, Prockop D, Horwitz E. 2006. Minimal criteria for defining multipotent mesenchymal stromal cells. The International Society for Cellular Therapy position statement. Cytotherapy 8(4):315-317.

Donega V, Nijboer CH, Braccioli L, Slaper-Cortenbach I, Kavelaars A, van Bel F, Heijnen CJ. 2014. Intranasal administration of human MSC for ischemic brain injury in the mouse: in vitro and in vivo neuroregenerative functions. PLoS One 9(11):e112339.

Eggenhofer E, Luk F, Dahlke MH, Hoogduijn MJ. 2014. The life and fate of mesenchymal stem cells. Front Immunol 5:148.

Faul F, Erdfelder E, Lang AG, Buchner A. 2007. G*Power 3: a flexible statistical power analysis program for the social, behavioral, and biomedical sciences. Behav Res Methods 39(2):175-191.

Fraser JK, Wulur I, Alfonso Z, Hedrick MH. 2006. Fat tissue: an underappreciated source of stem cells for biotechnology. Trends Biotechnol 24(4):150-154.

Fraser JK, Zhu M, Wulur I, Alfonso Z. 2008. Adipose-derived stem cells. Methods MolBiol 449:59-67.

Gholamrezanezhad A, Mirpour S, Bagheri M, Mohamadnejad M, Alimoghaddam K, Abdolahzadeh L, Saghari M, Malekzadeh R. 2011. In vivo tracking of 111In-oxine labeled mesenchymal stem cells following infusion in patients with advanced cirrhosis. Nucl Med Biol 38(7):961-967.

Gimble JM, Katz AJ, Bunnell BA. 2007. Adipose-derived stem cells for regenerative medicine. Circ Res 100(9):1249-1260.

Goodell MA, Rando TA. 2015. Stem cells and healthy aging. Science 350(6265):1199-1204.

Han S, Sun HM, Hwang KC, Kim SW. 2015. Adipose-Derived Stromal Vascular Fraction Cells: Update on Clinical Utility and Efficacy. Crit Rev Eukaryot Gene Expr 25(2):145-152.

Han SM, Han SH, Coh YR, Jang G, Chan Ra J, Kang SK, Lee HW, Youn HY. 2014. Enhanced proliferation and differentiation of Oct4- and Sox2-overexpressing human adipose tissue mesenchymal stem cells. Exp Mol Med 46:e101.

Hipp J, Atala A. 2008. Sources of stem cells for regenerative medicine. Stem Cell Rev 4(1):3-11.

Kapur SK, Dos-Anjos Vilaboa S, Llull R, Katz AJ. 2015. Adipose tissue and stem/progenitor cells: discovery and development. Clin Plast Surg 42(2):155-167.

Kern S, Eichler H, Stoeve J, KlÃ¼ter H, Bieback K. 2006. Comparative analysis of mesenchymal stem cells from bone marrow, umbilical cord blood, or adipose tissue. Stem Cells 24(5):1294-1301.

Kim WS, Park BS, Sung JH. 2009. Protective role of adipose-derived stem cells and their soluble factors in photoaging. Arch Dermatol Res 301(5):329-336.

Li Z, Hu X, Mao J, Liu X, Zhang L, Liu J, Li D, Shan H. 2015. Optimization of mesenchymal stem cells (MSCs) delivery dose and route in mice with acute liver injury by bioluminescence imaging. Mol Imaging Biol 17(2):185-194.

Lin G, Yang R, Banie L, Wang G, Ning H, Li LC, Lue TF, Lin CS. 2010. Effects of transplantation of adipose tissue-derived stem cells on prostate tumor. Prostate 70(10):1066-1073.

Ooi YY, Dheen ST, Tay SS. 2015. Paracrine effects of mesenchymal stem cells-conditioned medium on microglial cytokines expression and nitric oxide production. Neuroimmunomodulation 22(4):233-242.

Poglio S, De Toni-Costes F, Arnaud E, Laharrague P, Espinosa E, Casteilla L, Cousin B. 2010. Adipose tissue as a dedicated reservoir of functional mast cell progenitors. Stem Cells 28(11):2065-2072.

Poncelet AJ, Vercruysse J, Saliez A, Gianello P. 2007. Although pig allogeneic mesenchymal stem cells are not immunogenic in vitro, intracardiac injection elicits an immune response in vivo. Transplantation 83(6):783-790.

Schaffler A, Buchler C. 2007. Concise review: adipose tissue-derived stromal cells--basic and clinical implications for novel cell-based therapies. Stem Cells 25(4):818-827.

Seo MJ, Suh SY, Bae YC, Jung JS. 2005. Differentiation of human adipose stromal cells into hepatic lineage in vitro and in vivo. Biochem Biophys Res Commun 328(1):258-264.

Talens-Visconti R, Bonora A, Jover R, Mirabet V, Carbonell F, Castell JV, Gomez-Lechon MJ. 2006. Hepatogenic differentiation of human mesenchymal stem cells from adipose tissue in comparison with bone marrow mesenchymal stem cells. World J Gastroenterol 12(36):5834-5845.

Tarte K, Gaillard J, Lataillade JJ, Fouillard L, Becker M, Mossafa H, Tchirkov A, Rouard H, Henry C, Splingard M, Dulong J, Monnier D, Gourmelon P, Gorin NC, SensebÃ© L, Cellulaire StFadGdMeTr. 2010. Clinical-grade production of human mesenchymal stromal cells: occurrence of aneuploidy without transformation. Blood 115(8):1549-1553.

Teo AK, Vallier L. 2010. Emerging use of stem cells in regenerative medicine. Biochem J 428(1):11-23.

Trounson A, Thakar RG, Lomax G, Gibbons D. 2011. Clinical trials for stem cell therapies. BMC Med 9:52.

Varma MJ, Breuls RG, Schouten TE, Jurgens WJ, Bontkes HJ, Schuurhuis GJ, van Ham SM, van Milligen FJ. 2007. Phenotypical and functional characterization of freshly isolated adipose tissue-derived stem cells. Stem Cells Dev 16(1):91-104.

Wagner W, Wein F, Seckinger A, Frankhauser M, Wirkner U, Krause U, Blake J, Schwager C, Eckstein V, Ansorge W, Ho AD. 2005. Comparative characteristics of mesenchymal stem cells from human bone marrow, adipose tissue, and umbilical cord blood. Exp Hematol 33(11):1402-1416.

Wang L, Deng J, Tian W, Xiang B, Yang T, Li G, Wang J, Gruwel M, Kashour T, Rendell J, Glogowski M, Tomanek B, Freed D, Deslauriers R, Arora RC, Tian G. 2009. Adipose-derived stem cells are an effective cell candidate for treatment of heart failure: an MR imaging study of rat hearts. Am J Physiol Heart Circ Physiol 297(3):H1020-H1031.

Whone AL, Kemp K, Sun M, Wilkins A, Scolding NJ. 2012. Human bone marrow mesenchymal stem cells protect catecholaminergic and serotonergic neuronal perikarya and transporter function from oxidative stress by the secretion of glial-derived neurotrophic factor. Brain Res 1431:86-96.

Wu C, Li J, Pang P, Liu J, Zhu K, Li D, Cheng D, Chen J, Shuai X, Shan H. 2014. Polymeric vector-mediated gene transfection of MSCs for dual bioluminescent and MRI tracking in vivo. Biomaterials 35(28):8249-8260.

Yin L, Zhu Y, Yang J, Ni Y, Zhou Z, Chen Y, Wen L. 2015. Adipose tissue-derived mesenchymal stem cells differentiated into hepatocyte-like cells in vivo and in vitro. Mol Med Rep 11(3):1722-1732.

Ying C, Hu W, Cheng B, Zheng X, Li S. 2012. Neural differentiation of rat adipose-derived stem cells in vitro. Cell Mol Neurobiol 32(8):1255-1263.

Yukawa H, Watanabe M, Kaji N, Okamoto Y, Tokeshi M, Miyamoto Y, Noguchi H, Baba Y, Hayashi S. 2012. Monitoring transplanted adipose tissue-derived stem cells combined with heparin in the liver by fluorescence imaging using quantum dots. Biomaterials 33(7):2177-2186.

Zangi L, Margalit R, Reich-Zeliger S, Bachar-Lustig E, Beilhack A, Negrin R, Reisner Y. 2009. Direct imaging of immune rejection and memory induction by allogeneic mesenchymal stromal cells. Stem Cells 27(11):2865-2874.

Zhang Y, Liu N, Tang Y, Yang E, Dong S, Huang M, Pan C, Zhang Y, Zhang P, Chen H, Tang Z. 2014. Efficient generation of neural stem cell-like cells from rat adipose derived stem cells after lentiviral transduction with green fluorescent protein. Mol Neurobiol 50(2):647-654.

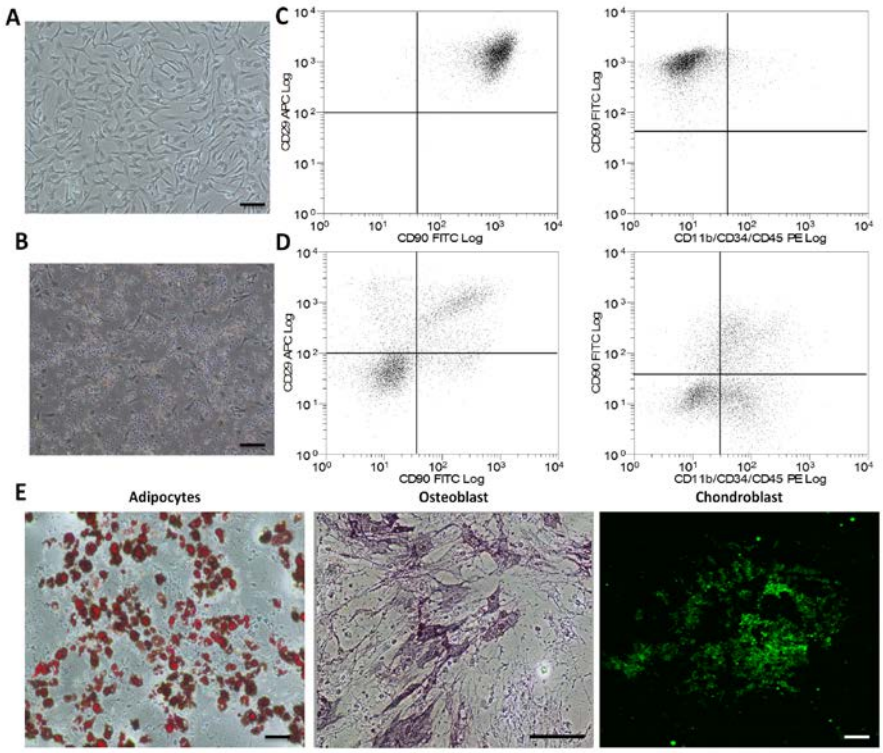

Figure 1

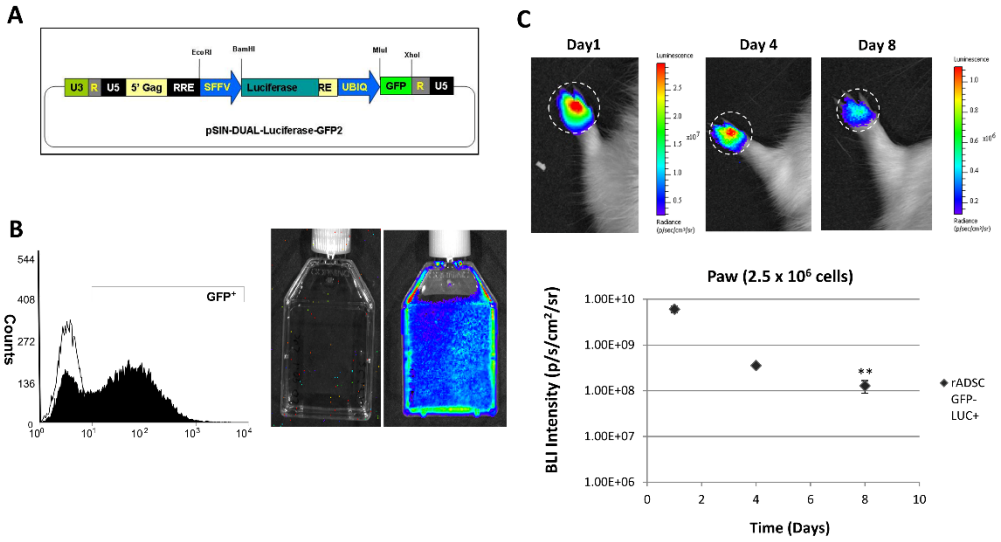

Figure 2

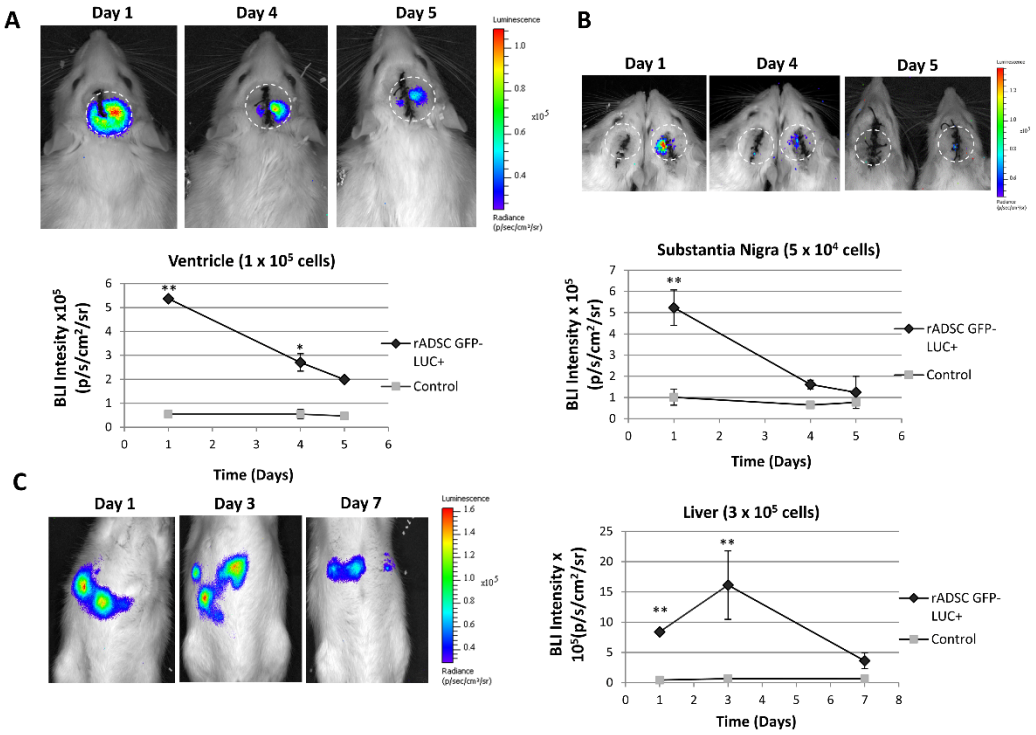

Figure 3

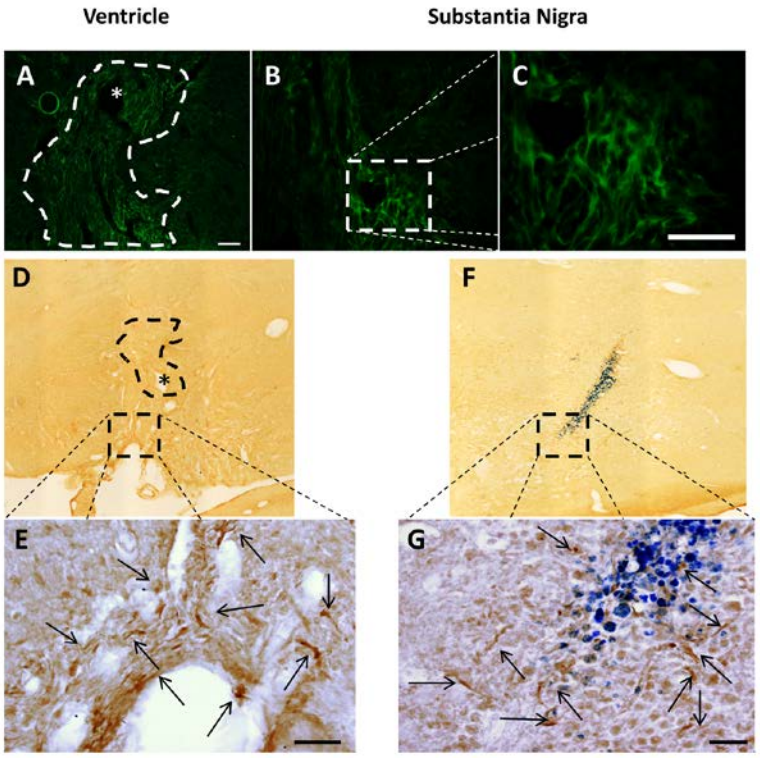

Figure 4

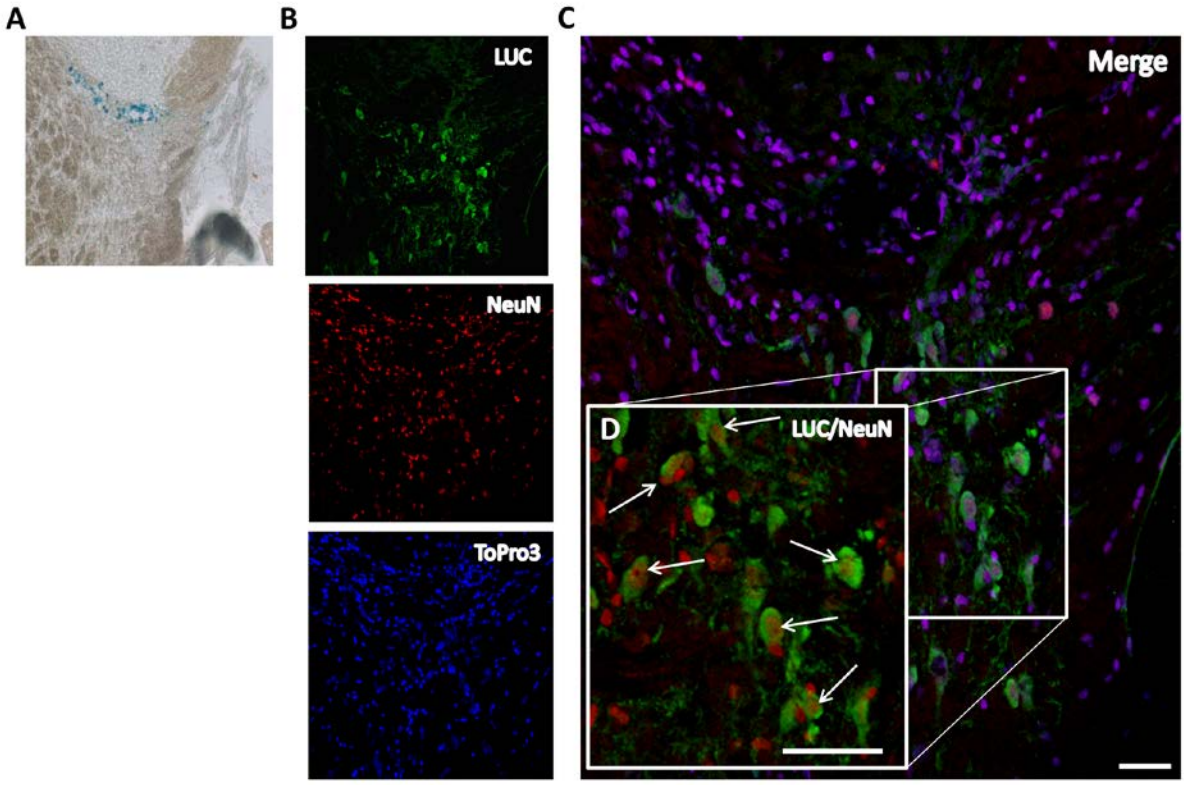

Figure 5

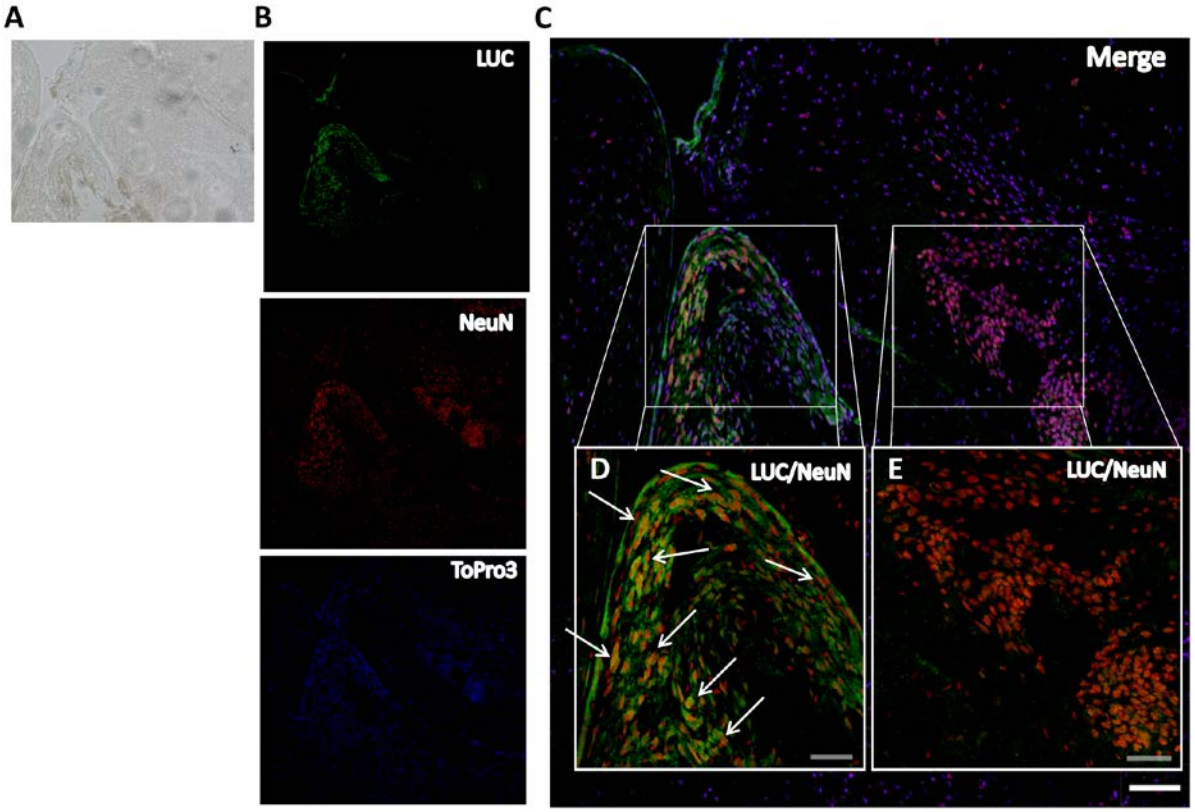

Figure 6

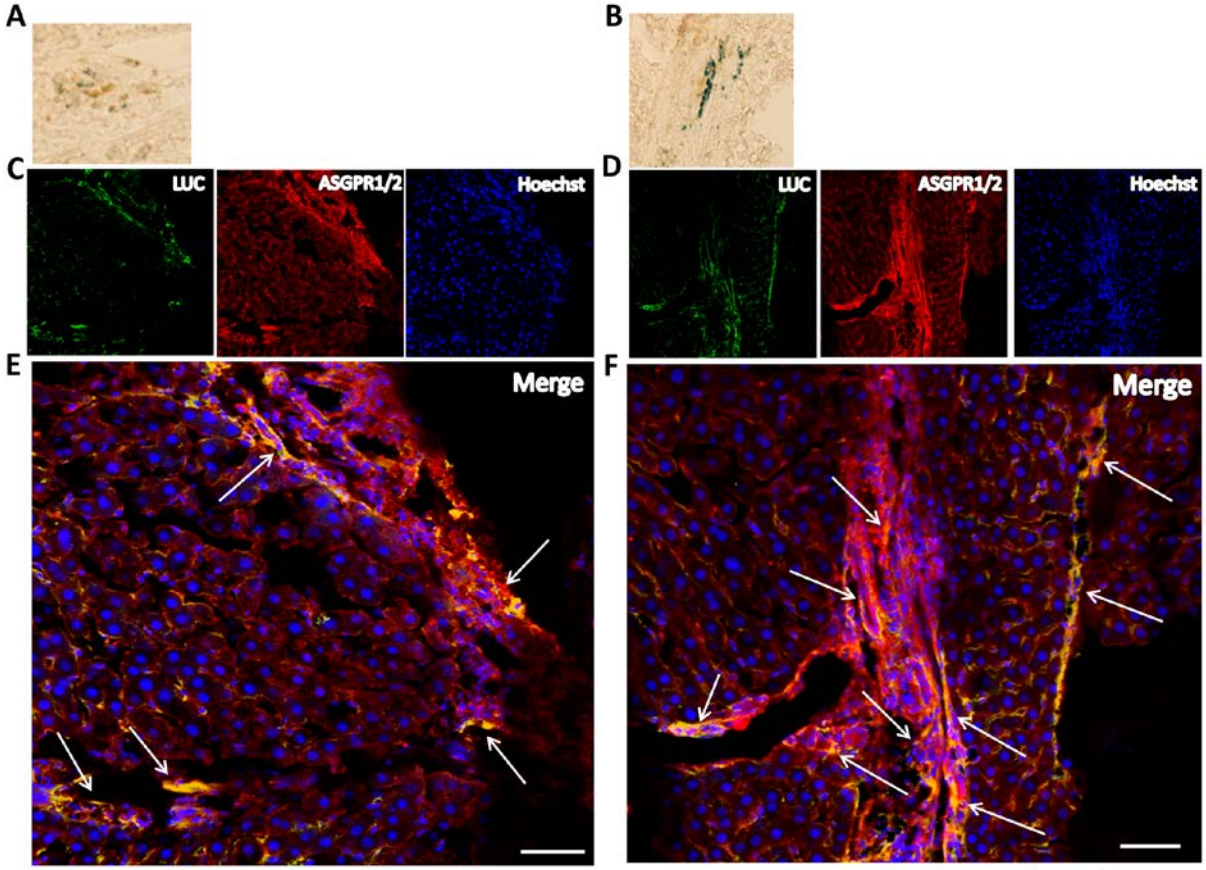

Figure 7

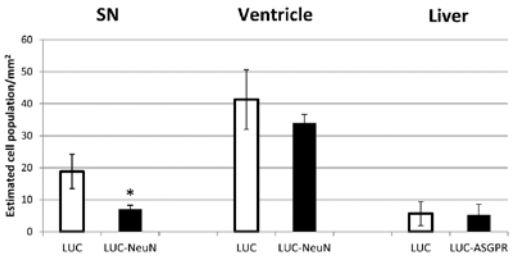

Figure 8